Journal of Molecular Structure 1178 (2019) 251–260

Contents lists available at ScienceDirect

Journal of Molecular Structure

journal homepage: http://www.elsevier.com/locate/molstruc

Solvothermal synthesis of zinc oxide nanoparticles: A combined experimental and theoretical study

Ankica Šarić [a, *], Ines Despotović [b], Goran Štefanić [a]

[a] Center of Excellence for Advanced Materials and Sensing Devices, Ruđer Bošković Institute, Bijenička 54, 10000 Zagreb, Croatia
[b] Division of Physical Chemistry, Ruđer Bošković Institute, Bijenička 54, 10000 Zagreb, Croatia

ARTICLE INFO

Article history:
Received 2 August 2018
Received in revised form
4 October 2018
Accepted 8 October 2018
Available online 11 October 2018

Keywords:
Nanostructured materials
Oxide materials
Density functional calculations
Optical properties
SEM
X-ray diffraction

ABSTRACT

Zinc oxide particles were synthesized from zinc acetylacetonate in the presence of triethanolamine (TEA) and various alcoholic solvent, ethanol or octanol, at 170 °C. The structural, optical and morphological characteristics of ZnO particles were monitored using X-ray powder diffraction (XRD), UV–Vis and FT-IR spectroscopies and field emission scanning electron microscopy (FE-SEM). The experimental findings were confirmed by means of DFT calculations which were obtained in nonpolar alcohol 1-octanol, as a follow up to our previous study in polar ethanol [9]. The nucleation and formation mechanism of ZnO nanoparticles is proposed considering the results obtained from a computational study of Gibbs free energies of ZnO–TEA molecular interactions (ΔG^*_{INT}) in various solvent system. The calculations revealed different binding affinities which initiated the nucleation processes of ZnO nanoparticles in the presence of alcohols of different size and polarity. The high chelating efficiency of TEA towards zinc with tetrahedral geometry is observed. The results of X-ray diffraction size-strain analysis indicate the presence of size anisotropy as well as a reduction in the ZnO crystallite size with the change of solvent from ethanol to 1-octanol (<10 nm).

1. Introduction

Zinc oxide is of interest in many applications as an important material with excellent combination of optical, electrical and microstructural properties. In order to optimize the properties of ZnO material for the highly technical or biomedical applications it is necessary to control its structure and morphology [1]. Many researchers focused their investigations on relationship between synthetic parameters and properties of the ZnO [1–4]. One of the most powerful synthesis routes is represented by nonhydrolytic routes in which surfactants in the reaction mixture provide excellent control over crystallite size, shape and dispersibility [4]. Demir et al. [5] described method to obtain ZnO nanoparticles of monodisperse size distribution via acid-catalyzed esterification of zinc acetate dihydrate with 1-pentanol. The catalytic effect of *p*-TSA accelerated the nucleation rate and generated smaller particles with narrower size distribution. It is well known that to synthesize uniform nanoparticles it is required to generate nuclei at same time.

Ethanolamine molecules play an important role as particle growth modifiers; they are complexing, assembling and structure-directing agents in the reaction system and significantly influence the morphology of ZnO particles [6–9]. Wang et al. [6] reported a facile synthesis of ZnO with different morphologies (flowerlike, spindlelike, swordlike, umbrellalike) via an ethanolamine-assisted hydrothermal process. The flowerlike ZnO displayed an enhanced photocatalytic performance as compared with other ZnO architectures, which may be due to specific site-selective photocatalytic behavior related to Zn sites [6]. However, non-aqueous systems offer the possibility of better control of the reaction mechanism and the rate of particle growth in comparison with aqueous system [3,8,10]. Contrary to methods with *ex situ* introduction of hydroxyl ions into the reaction system, which cause uncontrolled growth of ZnO nanoparticles, conversion of zinc precursors in organic solvents, allows the synthesis of nanomaterials with high crystallinity and well-defined uniform particle morphologies. It is well known that the one of the very important tasks was to avoid the influence of any external moisture to the system. Recently, Šarić et al. [11] investigated the esterification reaction for obtaining ZnO in highly anhydrous conditions and from zinc precursor without intrinsic water. The esterification reaction generated water molecules *in situ*

* Corresponding author.
E-mail address: asaric@irb.hr (A. Šarić).

https://doi.org/10.1016/j.molstruc.2018.10.025
0022-2860/

and can be considered as the initiation step of ZnO formation. Thus slowly released water molecules act as promoter of particle formation, including both nucleation and ZnO crystal growth. Wojnarowicz et al. [12–14] focused on the investigation of the significance of water in the microwave solvothermal synthesis of undoped and Co-doped ZnO NPs. The authors emphasized that by changing the water content in the precursor solution of hydrated zinc acetate in ethylene glycol, it is possible to control the size of both, undoped [12,14] and Co-doped [13] ZnO NPs. It is confirmed that an increase in the water content in precursor resulted in the increase in the size of obtained ZnO NPs, as a consequence of the change of quantity of the formed crystalline nuclei of ZnO to the remaining unreacted quantity of the zinc acetate [12–14]. Wojnarowicz et al. [12–14] proposed a size control growth mechanism of undoped and Co-doped ZnO nanoparticles.

Generally, nonaqueous routes can be distinguished as surfactant or solvent controlled preparation routes [10]. Many researchers [3,15–17] investigated the influence of a solvent on the ZnO formation in surfactant-free nonaqueous synthesis routes. Ambrožič et al. [3] proposed the formation mechanism of ZnO nanoparticles produced by starting from zinc acetylacetonate hydrate and 1-butanol or isobutanol. Tonto et al. [15] investigated the reaction mechanism of ZnO nanorods synthesized using the solvothermal esterification between zinc acetate and various alcohols in a series from 1-butanol to 1-decanol. The authors emphasized the interesting relationship between boiling point of the alcohol used and aspect ratio of ZnO nanorods, which increased from 1.7 to 5.6 when the alcohol was changed from 1-butanol to 1-decanol. On the other side, Bilecka et al. [18] studied the formation of ZnO nanoparticles in the presence of aromatic alcohol via a non-aqueous route by the use of benzyl alcohol. The formation mechanism of nanocrystalline ZnO particles from the reaction of zinc acetylacetonate with NaOH in ethanol was likewise investigated by Inubushi et al. [19].

Salavati-Niasari research group [20–25] investigated the influence of synthesis procedure on the formation and properties of ZnO nanomaterial and composites. Along with other physical and chemical properties the size and morphology of ZnO nanoparticles can be modified by using different routes of the synthesis. ZnO nanoflowers were synthesized from zinc oxalate without using additives by a fast microwave-assisted polyol method [23]. Also, Salavati-Niasari's research group reported synthesis of ZnO nanoparticles by solid-state reaction [20–22]. Solvent-free syntheses have recently attracted considerable attention in the field of green chemistry as novel and simple mechano-chemical solid-solid method [22]. Also, the solid-state thermal decomposition of zinc acetylacetonate was already utilized in the production of ZnO nanofibers and nanoparticles [24]. Notwithstanding the simplicity of this method, the mechanism of thermal decomposition of zinc acetylacetonate obtained by the sublimation process of $Zn(acac)_2$ powder is complex. This method can be developed to prepare various morphologies of metal oxides [24]. ZnO morphology has a significant influence on the optical properties of ZnO, as well as on the other semiconductor photocatalyst material [25].

Here we present new results obtained by the theoretical study, by means of quantum chemical calculations at the density functional theory level, related to ZnO nanomaterial synthesized in 1-octanol following our previously reported procedure [8]. This research is a follow up to our previous combined experimental and theoretical study of ZnO nanomaterial obtained in ethanol [9]. In a previous paper [9] we studied and compared the impact of a versatile family of ethanolamines (MEA and TEA) on the microstructural properties of the ZnO particles prepared in ethanol. The aim of present combined experimental and theoretical study is to better understand on a molecular level the mechanism which initiated the ZnO nucleation process continued by the growth of nanoparticles in the presence of alcohols of different size and polarity and TEA, as well as to improve the predictability of formation of nanoparticles and their aggregation.

2. Experimental

2.1. Materials and synthesis

Zinc acetylacetonate monohydrate ($Zn(C_5H_7O_2)_2 \cdot H_2O$; *Alfa Aeser*®), triethanolamine ($C_6H_{15}NO_3$; *Fisher Chemical*), absolute ethanol (C_2H_5OH; *J. T. Baker*) and 1-octanol ($CH_3(CH_2)_7OH$; *Sigma Aldrich*), all of analytical purity, were used for the preparation of samples. Commercial ZnO was supplied by *Ventron*.

Sample notation and the experimental conditions used for their preparation are given in Table 1 following our previously reported procedure [8]. In a typical synthetic procedure triethanolamine (TEA) was first dissolved in alcohol. Alcohols used in this research were ethanol (samples E) and 1-octanol (samples O). Then $Zn(acac)_2 \cdot H_2O$ was added to this solution and the molar ratio of TEA to $Zn(acac)_2 \cdot H_2O$ was adjusted to 1:2 and 1:1 (TEA/alcohol precursor solutions). Each precipitation system contained 0.5 g of $Zn(acac)_2$. Different amounts of TEA were dissolved in alcohol. Thus prepared transparent precursor solution was autoclaved at 170 °C for 4 or 24 h. A 50 mL Teflon-lined stainless steel autoclave was used. After autoclaving the precipitates were separated from supernatants by centrifugation, washed several times with ethanol and dried.

2.2. Measurements and characterization

Field Emission Scanning Electron Microscope (FE-SEM) model JSM-7000F, manufactured by *Jeol Ltd*. was used to examine the morphology and size of the particles. UV/Vis absorption spectra were recorded with a *Shimadzu* UV/Vis/NIR spectrometer equipped with an integrated sphere (model UV-3600). FT-IR spectra were recorded using a *Perkin Elmer* spectrometer (model 2000). The structure of samples was determined at room temperature by X-ray diffraction (XRD) using *Italstructures* X-ray powder diffractometer (APD 2000, Cu-K_α radiation, graphite monochromator, scintillation detector).

2.3. Size–strain line-broadening analysis

Size–strain line-broadening analysis of the ZnO samples was performed using the results of Williamson-Hall analysis [26]. The values of volume-averaged domain size (D_v) and the upper-limits of microstrains (e) were estimated from the results of Williamson-Hall analysis by using equation:

Table 1
The notation and experimental conditions used for the preparation of ZnO samples. Each precipitation system contained 0.5 g of $Zn(acac)_2$ [8]. Ageing temperature was 170 °C.

Sample	[TEA]/[Zn (acac)$_2$]	Ethanol/ml	Octanol/ml	t_{ageing}/h
E1	1:2	30		4
E2	1:2	30		24
E3	1:1	30		4
E4	1:1	30		24
O1	1:2		30	4
O2	1:2		30	24
O3[a]	1:1		30	4
O4	1:1		30	24

[a] There was no precipitation.

$$\left(\frac{\beta \cos\theta}{\lambda}\right) = \frac{K}{D_v} \times \left(\frac{4e \sin\theta}{\lambda}\right), \quad [1]$$

where λ is wavelength, β stands for the physical broadening of diffraction line and K is constant close to 0.9. The β values were obtained by convolution-fitting approach (program SHADOW [27]) in which the instrumental profile (diffraction lines of well-crystalline zincite powder) is convoluted with a refinable Voigt function to fit the observed profile.

2.4. Computational methods

All calculations were performed by means of quantum chemical calculations at the density functional theory (DFT) level using the Gaussian 09 program (revision D1) [28]. The M05-2X functional [29] designed by the Truhlar's group has been chosen. It provides very accurate thermodynamic parameters, being particularly successful in nonbonding interactions treatment [29–31], especially in reproducing geometries, dipole moments and homolytic bond energies in various zinc complexes [32,33]. The 6-31 + G(d,p) + LANL2DZ mixed basis set has been utilized. The Pople's 6-31 + G(d,p) double-ξ basis set was chosen for N, O, H atoms and the LANL2DZ basis (LANL2 pseudopotential for inner electrons and its associated double-ξ basis set (DZ)) was used for the transition-metal (Zn) atoms [34]. This gave rise to the M05-2X/6-31 + G(d,p) + LANL2DZ model utilized for geometry optimization which has been frequently used for studies of transition-metal containing systems. The geometric structures of the molecules were optimized by minimizing energies with respect to all geometrical parameters without imposing any molecular symmetry constraints and using a tight convergence condition. The Berny algorithm using redundant internal coordinates was employed. Frequency calculations were made under the harmonic approximation on all the optimized structures at the same level of theory with no scaling in order to confirm that the structures correspond to the true minima, meaning that no imaginary frequencies were present, as well as to extract thermal Gibbs free energy corrections. The final single point energies were obtained using a highly flexible 6-311++G(2df,2pd) basis set for the N, O, H atoms, while the same LANL2DZ ECP type basis set for zinc atoms was employed. The self-consistent field (SCF) calculations were conducted under a tight condition imposing the threshold value of 10^{-8} hartree to total energy difference during the iteration process. The integration grid in self-consistent field calculations was set to FineGrid having 75 radial shells and 302 angular points per shell. The 2-electron integral accuracy was set to 10^{-13}. The FoFCou algorithm with NoSymm option was used. All geometry optimizations, frequency calculations and single point energy evaluations were conducted by taking solvent effects into account. To evaluate the bulk solvent effects (1-octanol, $\varepsilon = 9.86$; ethanol, $\varepsilon = 24.85$) the implicit SMD polarizable continuum solvation model [35] has been employed. It represents a very practical approach to simulate the solvation environment and determine the effect of the medium on the structure and stability of solutes in a solution.

One of major difficulties in modelling the formation process of ZnO–TEA monomers, as well as their association into oligomers, is the correct sampling of the conformational space of molecules. Due to many different monomer structures, as well as their associate structures, optimization for a large number of different starting structures had to be performed in order to find the global minimum. In practice, different ways are utilized to create such starting structures. They are usually obtained by a low-level quantum-chemical method, or by an empirical force-field combined with molecular dynamics or Monte Carlo techniques, or using generic algorithms. Starting structures are also frequently build from literature data (X-ray data), or manually sampled by using chemical intuition. In this work the latter approach was used to generate the starting structure of the ZnO–TEA monomer as well as other oligomers. The conformational space was manually sampled for the ZnO–TEA monomer, taking into account various donor and acceptor sites of the ZnO and TEA molecule. The numbers of configurations were optimized, then the most stable ones were selected and further used as a starting point for building the dimers. The two most stable dimers were then associated directly into tetramers.

The Gibbs free energy of interaction, ΔG^*_{INT}, was computed using the supramolecular approach according to the simple formula:

$$\Delta G^*_{INT,AB} = G^*_{AB} - G^*_{A} - G^*_{B} \quad (1)$$

as the difference between the total free energy (G^*_{AB}) of the associates (ZnO–TEA, or their oligomers), and the sum of the total free energies ($G^*_A + G^*_B$) of the associating units A and B. The total free energy of the species in the liquid was computed using the expression

$$G^*_X = E^{Tot}_{soln} + \Delta G^*_{VRT,soln} \quad (2)$$

where the term E^{Tot}_{soln} corresponds to the basic energy of a density functional theory calculation using the SMD model, while the $\ddot{A}G^*_{VRT,soln}$ term encompasses vibrational, rotational and translational contribution to the solution free energy, being computed by applying the ideal gas partition functions to the frequencies calculated in the dielectric medium and the 1M standard state. A more negative value of the binding energy implied the more stable formed species. No BSSE correction to the binding energies has been applied.

The topological analysis of the charge density distribution using the Bader's quantum theory of atoms in molecules (QTAIM) [36] was performed by employing AIMALL software package [37] using the SMD/M05-2X/6-31 + G(d,p) + LANL2DZ wave function obtained from optimization. Within the QTAIM analysis the electron density was analyzed for two major characteristics including (a) the existence of critical points (CPs), which are special points where electron density exhibits maximum, minimum, or a saddle point in space, and (b) for the bond paths [38], the line of maximum electron density connecting two interacting atoms in the energetic minimum structure which indicates that the two atoms are bonded. The point of the minimum value of electron density along that line is called the bond critical point (BCP) and the value of topological parameters, such as electron density $\rho(r_c)$, Laplacian$\nabla^2\rho(r_c)$, electronic kinetic energy $G(r_c)$, electronic potential energy density $V(r_c)$, total energy density $H(r_c)$ at that point explain the features of interatomic interactions. $\nabla^2\rho(r_c) < 0$ indicates that the charge density is locally concentrated, while $\nabla^2\rho(r_c) > 0$ indicates that the charge density is locally depleted. The chemical bond nature can be described qualitatively concerning the signs and values of the electron density Laplacian $\nabla^2\tilde{n}(r_c)$ and of the electron energy density $H(r_c)$ at the corresponding bond critical point in accordance with the following criteria. The interactions characterized by $\nabla^2\rho(r_c) < 0$ and $H(r_c) < 0$ point to a shared interaction, i.e., weakly polar and nonpolar covalent bonds. On the other hand, the interaction characterized by $\nabla^2\rho(r_c) > 0$ and $H(r_c) > 0$ suggests the closed shell interactions such as weak hydrogen bonds, van der Waals interactions and ionic bonds. The intermediate interactions which include strong hydrogen bonds and most of the coordinate bonds are characterized by $\nabla^2\rho(r_c) > 0$ and $H(r_c) < 0$ [39,40]. A very high negative value of the $\nabla^2\rho(r_c)$ is an indication of a strong covalent bond, while a high positive value

corresponds to a strong noncovalent bond. The energies of the coordinate bonds (Zn—O, Zn—N) and of other intra- and intermolecular hydrogen bonds have been calculated by the Espinosa's equation

$$E = 0.5V(rc) \quad (7)$$

where E is the bond energy (a.u.), and $V(r_c)$ is potential energy density (a.u.) at the corresponding critical point [41]. The Espinosa's relationship is widely used for the energy estimation of different types of hydrogen [42,43], van der Waals [44] coordinate [45,46] and homopolar bonds [47].

3. Results and discussion

3.1. Microstructural analysis

The morphologies and microstructures of ZnO particles in as-synthesized samples (Table 1) [8] were examined with FE-SEM and XRD. Fig. 1 shows the SEM images of ZnO particles in sample O1 prepared in 1-octanol solution (a), and sample E1 prepared in ethanol solution (b), both obtained in the presence of small amount of TEA (mole ratio [TEA]/[Zn(acac)$_2$] = 1:2). Sample O1, prepared in octanol (Fig. 1a) consists mostly of small irregular spherical aggregates ~100 nm in size made up of loosely assembled nanoparticles (<20 nm). Alongside, the much smaller irregular nanoparticle aggregates are also visible. However, in the ethanol solution, there was no tendency of aggregation of fine uniform ZnO nanoparticles (<20 nm), as shown in the SEM image in Fig. 1b (sample E1). It seems that this experimental condition provided a sufficient combination of favourable electrostatic interaction between ZnO nanoparticles, polar molecules of ethanol and molecules of TEA to prevent particles from aggregating. The results of X-ray diffraction line-broadening analysis (Table 2) show that ZnO crystallites in sample O1 prepared in octanol solutions appear to be significantly smaller (~5 nm, $D_v\|c$-ax ~9 nm; microstrains $<2 \times 10^{-4}$) than in ethanol in sample E1 (~9 nm, $D_v\|c$-ax ~19 nm; microstrains $<2 \times 10^{-4}$).

However, the formation of bigger densely packed spheres (˃500 nm) assembled from fine and uniform ZnO nanoparticles is favoured by increasing the TEA concentration ([TEA]/[Zn(acac)$_2$] = 1:1) in both, polar ethanol and nonpolar octanol. Fig. 2 shows the SEM images of ZnO particles in sample O4 prepared in 1-octanol solution (a), and sample E4 prepared in ethanol solution (b), both obtained at the mole ratio [TEA]/[Zn(acac)$_2$] = 1:1. Sample O4, prepared in octanol (Fig. 2a) consists of the large compact spheres (˃500 nm) formed by the aggregation of several smaller spheres. The presence of ethanol along with TEA molecules at [TEA]/[Zn(acac)$_2$] = 1:1 also favoured the aggregation of ZnO nanoparticles into big regular spheres (˃500 nm) as shown in Fig. 2b and Fig. S1c, in comparison with freestanding ZnO nanoparticles prepared at the deficiency of TEA ([TEA]/[Zn(acac)$_2$] = 1:2) (Fig. 1b, Fig. S1b). Small nanoparticles (<20 nm) on the surface of spheres are well visible (Fig. 2a and b). It seems likely that an increase in TEA concentration could potentiate TEA coating on ZnO nanoparticles, which allowed for the nanoparticles to attach to each other more tightly and favoured the formation of big ZnO spheres. The difference in these processes might be explained by different interactions of the solvent molecules with the surface of nanoparticles.

Table 2
Estimated values of the volume averaged domain sizes (D_v) and upper limits of microstrains (e) and the corresponding values in the directions parallel to the c-ax of zincite lattice as determined from the results of diffraction line broadening [8] (Williamson-Hall analysis).

Sample	D_v/nm	$e \times 10^3$	$D_v\|c$-ax/nm	$e \times 10^3\|c$-ax
E1	9 (1)	0.6 (2)	19 (2)	<0.2
E2	12 (1)	0.6 (2)	21 (2)	<0.2
E3	7 (1)	<0.2	12 (2)	1.5 (2)
E4	9 (1)	0.3 (2)	21 (2)	1.6 (2)
O1	5 (1)	0.3 (2)	9 (1)	<0.2
O2	7 (1)	<0.2	14 (1)	1.1 (2)
O4	7 (1)	1.0 (2)	16 (1)	<0.2

The results of X-ray diffraction line-broadening analysis show that ZnO crystallites in sample O4 prepared in octanol solutions appeared to be smaller (~7 nm, $D_v\|c$-ax ~16 nm; microstrains $<2 \times 10^{-4}$) than in ethanol in sample E4 (~9 nm, $D_v\|c$-ax ~21 nm; microstrains 1.6×10^{-3}, Table 2). The results of XRD analysis are summarized in Table 2 and Fig. 3. XRD measurements showed that in all samples ZnO was present as a single phase. Fig. 3 shows characteristic XRD patterns of samples O2, O4, E2, E4 and Fig. S2 XRD patterns of samples O1, E1 and E3. The results of our previously obtained [8] Williamson-Hall analysis are summarized in Table 2. The results of individual profile fitting (program XFIT) indicated presence of size anisotropy with significantly narrower diffraction lines along the direction ⟨00l⟩ (Fig. 2). Therefore, we separately estimated D_v and e values in the direction parallel to c-ax from the β values of the diffraction lines 002 and 004. In summary, the results of XRD analysis show that for the same experimental conditions the change of solvent from octanol to ethanol caused a reduction in the ZnO crystallite size (Table 2, Fig. 3). Long-chain alcohols were introduced by Park et al. [48], as solvents which were expected to decrease the overall polarity of the system and to provide a repulsive force between particles. The authors concluded that the lowered polarity decreased the solubility of small

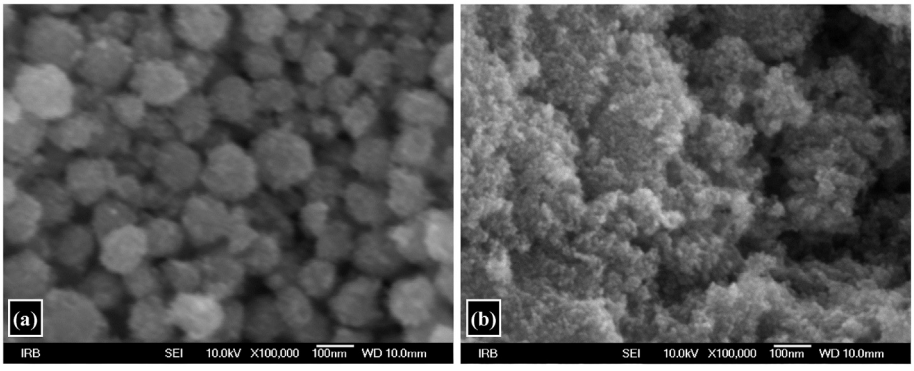

Fig. 1. FE-SEM images of samples: (a) O1, (b) E1.

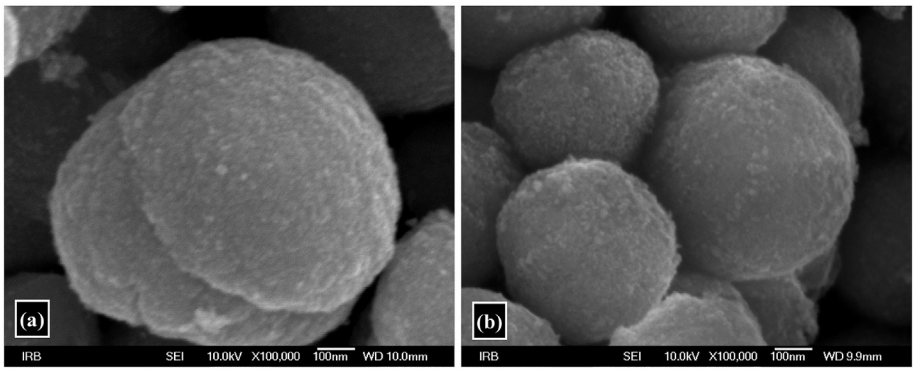

Fig. 2. FE-SEM images of samples: (a) O4, (b) E4.

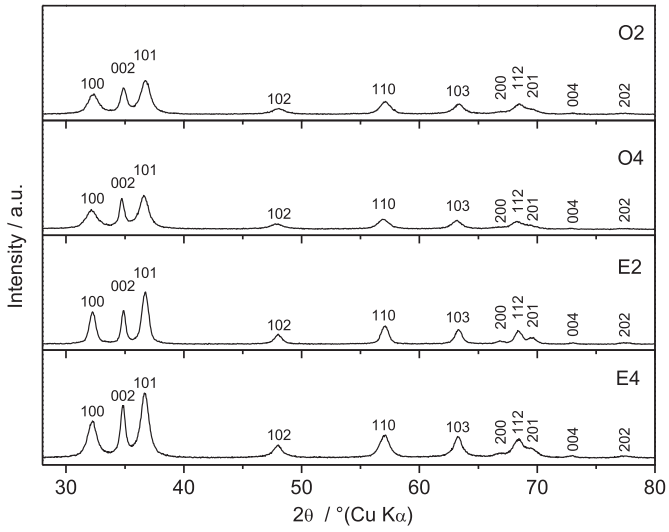

Fig. 3. X-ray diffraction patterns of samples O2, O4, E2 and E4.

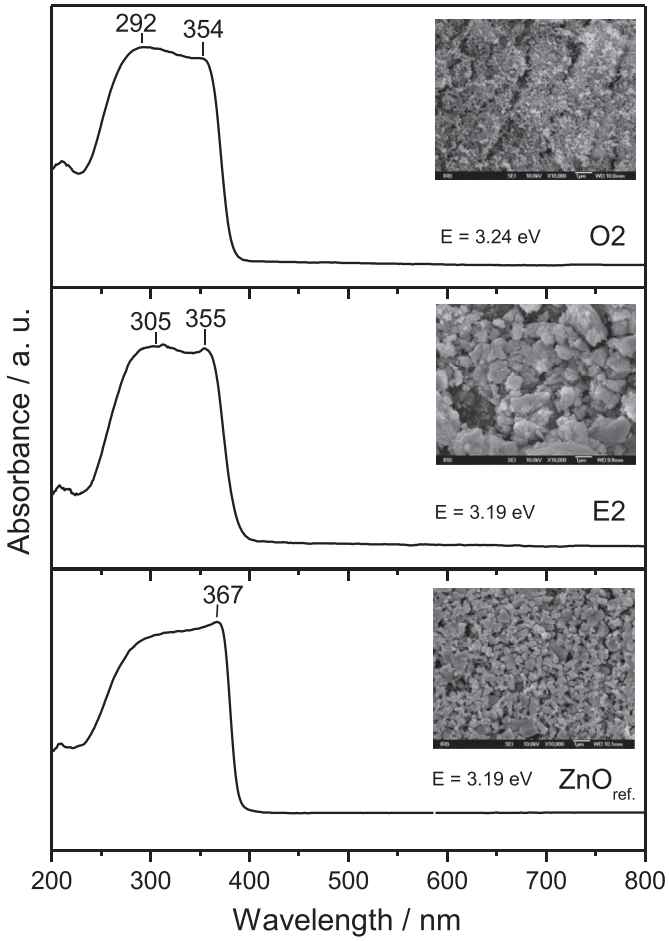

Fig. 4. UV–Vis spectra of samples O2, E2, and reference ZnO. Inset images show the corresponding SEM images at the same magnification (10000 ×) and calculated band gap values.

oligomers in the system, which shortens the turbidity time. From the relationship between the dielectric constant and turbidity time it can be concluded that the reaction participating units are small oligomers rather than monomers [48]. Sadasivan et al. [49] also observed similar results. The authors concluded that the steric hindrance may be predominant factor for lower alcohols, weaker hydrogen bonding predominant one for the higher alcohols. Namely, a weaker hydrogen bonding between solvent molecules and nucleophile enhance the rate of hydrolysis, while the steric hindrance of an alkyl group expressed through higher solvent viscosity for higher alcohols slow down the rate of hydrolysis [49]. The authors concluded that the final particle size depend on the solvent polarity [48,49]. Triethanolamine (TEA) molecules play important roles as complexing, assembling and structure directing ligands in the precursor solution probably as coordinated ions $[Zn(TEA)_x]^{2+}$ or $[ZnO(TEA)_x]$ (besides remaining $(Zn(OH)_2$, $[(Zn(OH)_4]^{2-}$ and Zn^{2+}) which limits the existence of free zinc ions and controls the ZnO nuclei formation.

3.2. UV–Vis and FT-IR spectroscopies

The optical absorbance spectra of ZnO particles are shown in Fig. 4. Fig. 4 shows the UV–Vis spectra of selected samples and the reference ZnO material, their corresponding particle morphologies (inset) and calculated band gap values. As can be seen, the as prepared powder, as well as reference ZnO, had no optical absorption in the visible region, but there was good absorption nearly in the whole UV region. The UV–Vis spectra of ZnO samples, as well as commercial ZnO, are characterized by broad and intensive absorption between 400 and 200 nm. The band gap values were obtained using the procedure described by Dharma and Pisal [50]. One can see from Fig. 4 that the as prepared sample in octanol (O2) solution show a UV absorption edge which is blue-shifted with respect to the absorbance of reference ZnO material. It is attributed

to the size induced change of ZnO band gap energy. The relationship between the particle size and optical properties of ZnO nanoparticles was recently reported [51]. ZnO morphology has a significant influence on the optical properties of ZnO, as well as on the other semiconductor photocatalyst material. Among the various semiconductor photocatalyst material nanostructured $Zn_3V_2O_8$ has attracted significant consideration for degradation of anionic and cationic dyes under UV irradiation in a short time [25].

Fig. S3 shows characteristic parts of the FT-IR spectra of all ZnO samples. The right panel shows the spectra of samples synthesized in the presence of octanol (O1, O2 and O4), whereas the left panel shows the FT-IR spectra of samples synthesized in the presence of ethanol (E1, E2, E3 and E4). The FT-IR bands between 540 and 397 cm^{-1} with two poorly resolved bands are characteristic of ZnO. Besides, the FT-IR spectra of ZnO samples are characterized by the bands above 600 cm^{-1} due to the adsorbed water and organic molecules. The IR band at ~1630 cm^{-1} can be attributed to the bending vibration of H_2O molecules adsorbed on ZnO particles. The FT-IR bands at 1582 to 1619 cm^{-1}, as well as the bands at 1385 to 1414 cm^{-1}, can be attributed to the stretching vibration of chemisorbed C=O bands originating from acetylacetonate [8]. The presented FT-IR spectra indicate chemisorptions of carbonyl and carbonate groups on the surface of ZnO nanoparticles.

3.3. The mechanism of ZnO particle formation

The formation of final ZnO particles can be considered in several sequential steps: (1) monomer formation, (2) nucleation, (3) crystal growth, and (4) possibly aggregation of ZnO nanoparticles. The presence of triethanolamine in alcoholic solvent of different size and polarity, had a significantly different influence on the all steps, nucleation as well as on the crystal growth and aggregation of ZnO nanoparticles. Triethanolamine combines the properties of amines as weak bases and alcohols with three hydroxyl chains. Due to special ability of TEA to participate in reactions common to both groups, the spontaneous nucleation and growth of ZnO nanoparticles was limited.

On the basis of both microstructural and theoretical studies, the nucleation and growth mechanism of ZnO nanoparticles is proposed. Based on the results obtained by means of quantum chemical calculations at the density functional theory level, it was established that the nucleation kinetics and ZnO nanoparticles growth, in the presence of TEA as a particles growth modifier and alcoholic solvent of different size and polarity, are strongly dependent on the properties of alcohol. The nucleation and formation mechanism of ZnO nanoparticles was proposed considering the results obtained from a computational study of Gibbs free energies of ZnO–TEA molecular interactions (ΔG^*_{INT}) in 1-octanol and our previously reported results in ethanol [9]. The calculations revealed different binding affinities which initiated the nucleation processes of ZnO into nanoparticles in the presence of alcohols of different size and polarity. These processes involve noncovalent interactions such as coordinate bonding, hydrogen bonding, van der Waals forces, electrostatic forces, etc. Here, as a follow-up to our previous investigations [9] performed in the presence of polar ethanol solvent, we systematically studied and compared all noncovalent interactions involved in the processes of nucleation and ZnO nanoparticle growth in the presence of nonpolar octanol solvent.

It is interesting to relate the structural motif for both most stable isolated ZnO–TEA monomers obtained in the presence of one polar [9] or the other nonpolar alcohol, as well as calculated values of Gibbs free energies of interactions for their formation (Fig. 5, Table 3). It is noticed that the structural motif for ZnO–TEA monomer (Fig. 5a) obtained in the presence of 1-octanol doesn't correspond to the motif of ZnO–TEA monomer obtained in ethanol [9] (Fig. 5b). Namely, when a ZnO–TEA monomer was formed, all three TEA hydroxyl chains could be attached to the ZnO molecule in different ways depending on the type of alcohol used (shown in Fig. 5 as ZnO–TEA(octanol) or ZnO–TEA(ethanol)).

To sum up, in the most stable conformation of isolated ZnO–TEA monomers obtained in both polar ethanol or nonpolar octanol, the strongest binding was accomplished via a similar coordinate bond, initiated with a characteristic ionic–dipolar interaction between hydrogen atoms from the OH group in TEA and oxygen in ZnO, which resulted in hydrogen atom transferring from the OH group on oxygen to ZnO. As a consequence of this process a lone electron pair on the oxygen atom from the OH group was involved in a new exceptionally strong coordinate bond with zinc (ZnO–TEA(ethanol) [9]: $d_{Zn-O} = 1.948$ Å, $E_{Zn-O} = -38.0$ kcal mol^{-1}; ZnO–TEA(octanol): $d_{Zn-O} = 1.954$ Å, $E_{Zn-O} = -37.5$ kcal mol^{-1}). The Zn–O bond is attributed to an intermediate type of interaction according to $\nabla^2\rho(r_c) > 0$ and $H(r_c) < 0$. It is more of an ionic type as indicated by the higher positive value of $\nabla^2\rho(r_c)$ compared with a corresponding value in the Zn–N bond. Namely, in the most stable ZnO–TEA monomers in both ethanol and 1-octanol a free electron pair on the nitrogen atom was involved in the coordinate bond with zinc (ZnO–TEA(ethanol) [9]: $d_{Zn-N} = 2.257$ Å, $E_{Zn-N} = -17.9$ kcal mol^{-1}; ZnO–TEA(octanol): $d_{Zn-N} = 2.246$ Å Å, $E_{Zn-N} = -18.6$ kcal mol^{-1}). The critical point of the Zn–N bond was characterized by the positive values of electron density Laplacian $\nabla^2\rho(r_c) > 0$ and by negative value of electron energy density $H(r_c) < 0$ indicating this type of interaction also as intermediate which is a feature of the coordinate bond. However, the most important binding responsible for additional stabilization of the most stable ZnO–TEA(octanol) monomer in comparison to ZnO–TEA(ethanol) monomer was accomplished via a newly coordinate bond where a free electron pair on the oxygen atom from the second remaining free TEA hydroxyl group was involved in bonding with zinc ($d_{Zn-O} = 2.2231$ Å, $E_{Zn-O} = -16.7$ kcal mol^{-1}), being more stabilized by strong O–H···O hydrogen bond between the hydrogen atom from remaining free TEA hydroxyl group and oxygen in ZnO ($d_{O \ldots H} = 1.563$ Å, $E_{O \ldots H} = -18.9$ kcal mol^{-1}, see Fig. 5a). Differently, the most stable ZnO–TEA(ethanol) monomer was stabilized by the weaker bifurcated O–H···O hydrogen bonds between the hydrogen atoms from both remaining free TEA hydroxyl groups and oxygen in ZnO ($d_{O \ldots H} = 1.644$ Å, $E_{O \ldots H} = -13.7$ kcal mol^{-1} and $d_{O \ldots H} = 1.677$ Å, $E_{O \ldots H} = -12.1$ kcal mol^{-1}, see Fig. 5b [9]). It is important to emphasize that the most stable ZnO–TEA monomer obtained in the presence of octanol possess stronger coordination ability which could replace weaker hydrogen bonds obtained in ethanol media. Obviously, the synergistic effect of all the above mentioned noncovalent interactions was present. The formation of such completely enclosed structure of ZnO–TEA(octanol) monomer in nonpolar alcohol was a consequence of the exceptional flexibility of all three of TEA hydroxyl chains compared to ethanol media. The calculated value of the Gibbs free energy interaction obtained in nonpolar octanol suggested that the amount of especially stable ZnO–TEA(octanol) monomer with $\Delta G^*_{INT} = -62.50$ kcal mol^{-1} was found to be the main controlling parameters for both nucleation and growth of ZnO nanoparticles, being 10.5 kcal mol^{-1} more stable than ZnO–TEA(ethanol) monomer with $\Delta G^*_{INT} = -51.50$ kcal mol^{-1} [9]. Moreover, when all is considered, the tetrahedral geometry in ZnO–TEA(octanol) monomer which increases zinc stability, as well as the ΔG^*_{INT} of its formation, one might conclude that in the presence of nonpolar octanol monomers found to imply most important parameters which initiated the nucleation processes of ZnO nanoparticles.

Furthermore, the formation of most stable dimer from the association of most stable monomers provide evidence of coordinate

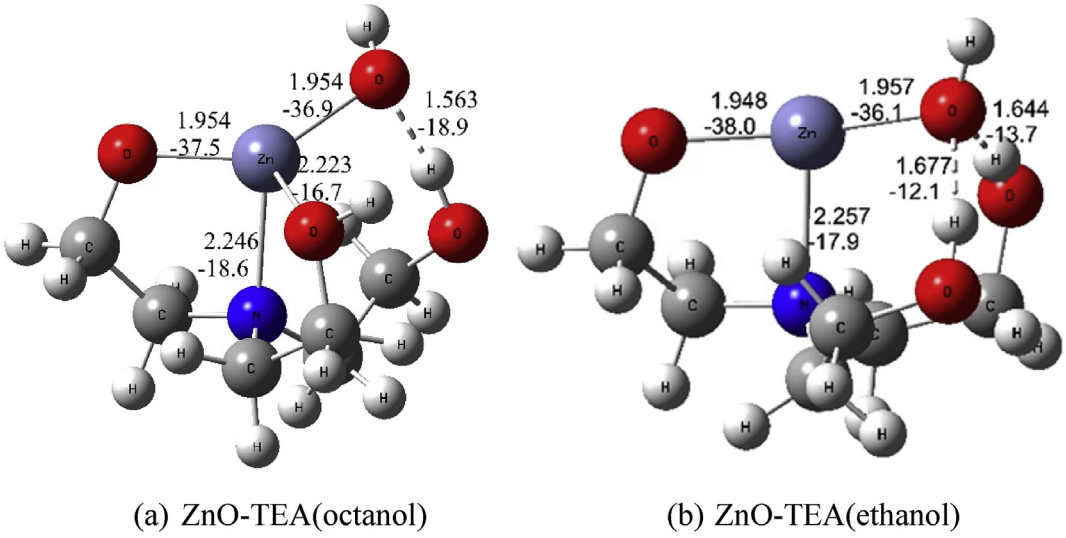

Fig. 5. The most stable structures of (a) ZnO–TEA monomers in 1-octanol and (b) ZnO–TEA monomers in ethanol (selected values of bond distances in Å and bond energies in kcal mol^{-1}).

Table 3
Formation of the most stable ZnO–TEA monomers[a] and their oligomers[b], and ZnO–TEA–ZnO species[c] in 1-octanol and ethanol [9]. Standard state (1M) free energies of interaction in 1-octanol and ethanol ΔG^*_{INT} computed by using the SMD solvation model at the M05-2X/6-311++G(2df,2pd) + LANL2DZ//M05-2X/6-31 + G(d,p) + LANL2DZ level of theory (in kcal mol^{-1}).

species ZnO–TEA (octanol)	ΔG^*_{INT}	species ZnO–TEA (ethanol)	ΔG^*_{INT} [9]
ZnO–TEA (octanol)	−62.5	ZnO–TEA (ethanol)	−51.5
$(ZnO–TEA)_2$(octanol)	−10.5	$(ZnO–TEA)_2$(ethanol)	−11.5
ZnO–TEA–ZnO(octanol)	−63.2	ZnO–TEA–ZnO(ethanol)	−28.3
$(ZnO–TEA)_4$(octanol)	8.2	$(ZnO–TEA)_4$(ethanol)	5.8

[a] According to the reaction: ZnO + TEA→ ZnO–TEA.
[b] According to the reaction for dimer: ZnO–TEA + ZnO–TEA → $(ZnO–TEA)_2$ and for tetramer: $(ZnO–TEA)_2$ + $(ZnO–TEA)_2$ → $(ZnO–TEA)_4$.
[c] According to the reaction for ZnO–TEA–ZnO species: ZnO–TEA + ZnO → ZnO–TEA–ZnO.

bonding via free electron pair on oxygen atoms with zinc atoms, having the same structural motif for the both most stable $(ZnO–TEA)_2$(octanol) and $(ZnO–TEA)_2$(ethanol) dimers, having closely followed the values of Gibbs energies, $\Delta G^*_{INT} = -10.5$ kcal mol^{-1} and $\Delta G^*_{INT} = -11.5$ kcal mol^{-1} [9] (Fig. 6, Table 3). Thanks to high chelating efficiency of triethanolamine towards zinc, a same tetrahedral geometry which increased its stability was noticed in both $(ZnO–TEA)_2$(octanol) (Fig. 6a) and $(ZnO–TEA)_2$(ethanol) (Fig. 6b, [9]) dimers. The advantages of association of a ZnO–TEA(ethanol) monomers during the formation of $(ZnO–TEA)_2$(ethanol) dimer should be emphasized in comparison to the association of a ZnO–TEA(octanol) monomers into dimer due to higher energetic requirements during the process of dimerization in octanol media, which involve at first an additional step of releasing one of the coordinate bonds in especially stable

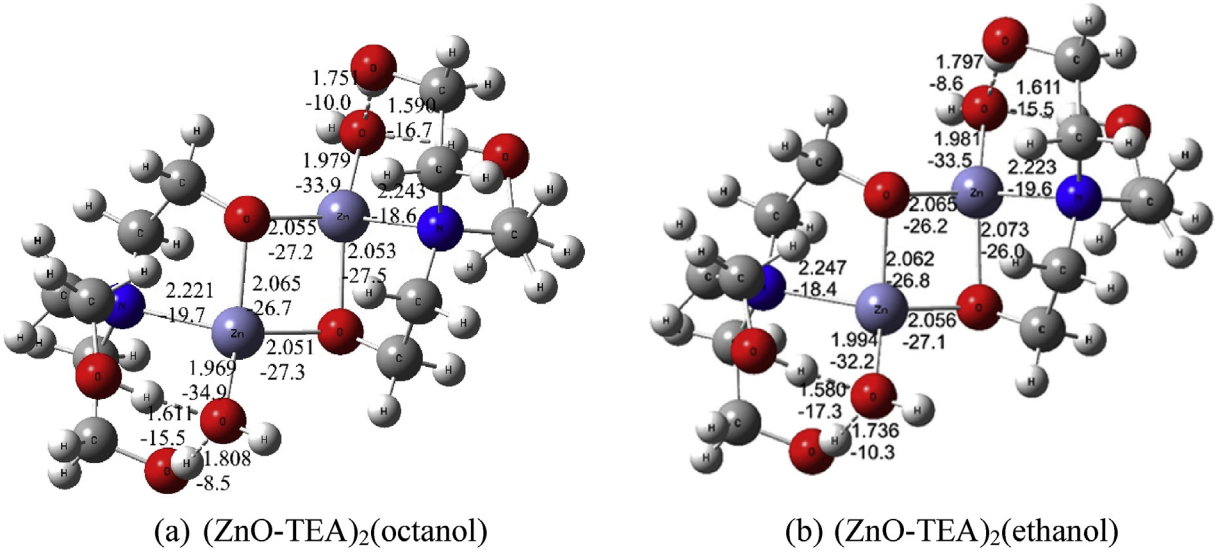

Fig. 6. The most stable structures of (a) $(ZnO–TEA)_2$ dimers in 1-octanol and (b) $(ZnO–TEA)_2$ dimers in ethanol (selected values of bond distances in Å and bond energies in kcal mol^{-1}).

monomeric structure. On the other hand, the possibility of the process of releasing one of the coordinate bonds in especially stable ZnO–TEA(octanol) monomer, as well as its potential dimerization, is also expected to be dependent on the access of other species with stronger coordination ability, as in the example at the excess amount of zinc salt. Namely, it is important to note the large capacity of the ZnO–TEA(octanol) monomer to attract other ZnO molecule when it's in excess ([TEA]/[$Zn(acac)_2$] = 1:2]), via coordinate bonding of free electron pairs on oxygen atoms with atoms zinc, which was accompanied by the formation of ZnO–TEA–ZnO(octanol) species. The tetrahedral structural motif of ZnO–TEA–ZnO(octanol) (Fig. 7a) species corresponds to the motif of the $(ZnO–TEA)_2$(octanol) dimer (Fig. 6a). Interestingly, supplementary adding of ZnO molecule to the isolated ZnO–TEA(octanol) monomer increased the stability of the system yielding the especially stable species ZnO–TEA–ZnO(octanol) with $\Delta G^*_{INT} = -63.2$ kcal mol^{-1}, being 1.2 kcal mol^{-1} even more stable than the existing ZnO–TEA(octanol) monomer and 52.7 kcal mol^{-1} more stable than the $(ZnO–TEA)_2$(octanol) dimer with $\Delta G^*_{INT} = -10.5$ kcal mol^{-1} (Table 3). However, as shown in Fig. 7, the structural motif for most stable ZnO–TEA–ZnO(octanol) species doesn't correspond to the motif of ZnO–TEA–ZnO(ethanol) species, having very big difference in values of Gibbs energies, $\Delta G^*_{INT} = -63.2$ kcal mol^{-1} and $\Delta G^*_{INT} = -28.3$ kcal mol^{-1} [9]. The higher chelating efficiency of TEA towards zinc with tetrahedral geometry is observed with the change of solvent from ethanol to octanol. Despite the mentioned differences related to octanol media, the most stable species of ZnO–TEA–ZnO(ethanol) with $\Delta G^*_{INT} = -28.3$ kcal mol^{-1}, being 16.8 kcal mol^{-1} more stable than the existing $(ZnO–TEA)_2$(ethanol) dimer with $\Delta G^*_{INT} = -11.5$ kcal mol^{-1} was found to imply important process parameters in controlling the ZnO nanoparticles nucleation at the excess amount of zinc salt in ethanol media [9]. It is interesting to note that the precipitation of ZnO was delayed for at least 4 h (it occurred after 24 h of ageing) at the mole ratio [TEA]/[$Zn(acac)_2$] = 1:1] solely in octanol media, indicating the strong impact of three TEA chains in such nonpolar media [8]. It seems that it is not possible to predict mechanisms responsible for nucleation and preferential growth of ZnO nanoparticles only from the knowledge of the most thermodynamically stable prenucleation intermediate.

The observed results point to a different formation mechanism of ZnO–TEA intermediates which initiated the nucleation processes of ZnO nanoparticles in the presence of alcohols of different size and polarity and at different molar ratio [TEA]/[$Zn(acac)_2$]. Based on the results obtained by the theoretical study which was in excellent agreement with the experimental microstructural study, it was established that the presence of solvent of different size and polarity had a strong impact on the ZnO nucleation process as well as crystal growth. To sum up, the use of 1-octanol as a nonpolar solvent leads to ZnO crystallites smaller than those obtained using polar ethanol. The results of X-ray diffraction line-broadening analysis show that for the same experimental conditions ZnO crystallites prepared in octanol solutions in the presence of small amount of triethanolamine ([TEA]/[$Zn(acac)_2$] = 1:2]) appeared to be significantly smaller (~5 nm) than in ethanol (~9 nm) both obtained in same experimental conditions [8]. This could be attributed to the spontaneous formation of ZnO–TEA intermediates ($\Delta G^*_{INT}<0$) which initiated the nucleation processes and plays a crucial role in the growth kinetics of ZnO nanoparticles. Calculated Gibbs free energies of ZnO–TEA molecular interactions revealed that the use of octanol as solvent leads to more spontaneous formation of ZnO–TEA monomers, as well as ZnO–TEA–ZnO species in comparison to ethanol solvent, which results in a higher nucleation rate of ZnO nuclei. It is well known that nucleation and growth are competitive processes. Therefore, the higher concentration of the initial nuclei results in smaller ZnO nanoparticles. The influence of solvents on the nucleation and growth of ZnO nanoparticles was studied in a series of alcohols from ethanol to 1-hexanol [16,17]. Changing the solvent from hexanol to ethanol indicate an increase of time required for nucleation and growth. Nucleation and growth are retarded in ethanol and 1-propanol in comparison to longer chain alcohols where nucleation and growth are fast. The solubility of the ZnO particles increases with increasing dielectric constant of the solvent [17]. This dependence indicates that the partially covalent bonding in ZnO is an important factor for determining the dissolution mechanism. Namely, for a purely ionic solid it would be expected that the solubility increases with increasing of the solvent dielectric constant.

Furthermore, possible formation of other kinds of stable oligomers, i. e. the most stable tetramer of $(ZnO–TEA)_4$ in both, octanol or ethanol solvent (Figure S4), from the association of two most stable $(ZnO–TEA)_2$ dimers implies a species for which the association process is endergonic ($\Delta G^*_{INT}>0$). Here, only the free hydroxyl groups from one $(ZnO–TEA)_2$ dimer could be attracted to free hydroxyl groups of other neighbouring $(ZnO–TEA)_2$ dimers by several bifurcated O–H···O hydrogen bonds, giving most stable tetramers

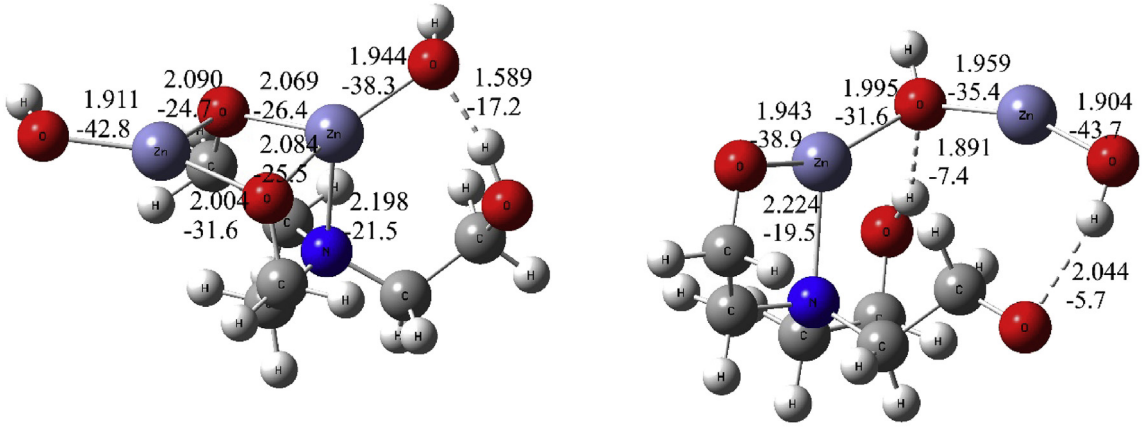

(a) ZnO-TEA-ZnO(octanol) (b) ZnO-TEA-ZnO(ethanol)

Fig. 7. The most stable structures of (a) ZnO–TEA–ZnO species in 1-octanol and (b) ZnO–TEA–ZnO species in ethanol (selected values of bond distances in Å and bond energies in kcal mol^{-1}).

of (ZnO–TEA)$_4$(ethanol) (Figure S4b) with $\Delta G^*_{INT} = 5.8$ kcal mol^{-1} [9], and (ZnO–TEA)$_4$(octanol) (Figure S4a) with $\Delta G^*_{INT} = 8.2$ kcal mol^{-1}. Due to hydrogen type of bonding, the advantages of association of (ZnO–TEA)$_2$ dimers during the formation of (ZnO–TEA)$_4$ tetramers should be emphasized in polar ethanol related to nonpolar octanol.

4. Conclusions

In this research paper in a combined experimental and theoretical study we presented impacts of alcohols of different size and polarity and different molar ratio [TEA]/[Zn(acac)$_2$] on the nucleation and growth mechanism of ZnO nanoparticles. Here, we present new results obtained by the theoretical study, by means of DFT calculations, related to ZnO nanomaterial synthesized in nonpolar alcohol 1-octanol, as a follow up to our previous study in polar ethanol [9]. The main part of the manuscript comprises a theoretical study based on DFT calculations which are in agreement with the experimental microstructural study.

Based on the results of, both microstructural and theoretical studies, the nucleation and growth mechanism of ZnO nanoparticles is proposed. The results obtained by means of quantum chemical calculations at the density functional theory level are in excellent agreement with the experimental microstructural study. It was established that the kinetics of nucleation and ZnO nanoparticles growth in the presence of TEA as particles growth modifier and alcoholic solvent of different size and polarity are strongly dependent on the properties of alcohol. The observed results point to a different formation mechanism of ZnO–TEA intermediates which initiated the nucleation processes of ZnO nanoparticles in the presence of alcohols of different size and polarity and at different molar ratio [TEA]/[Zn(acac)$_2$]. The calculations revealed different binding affinities which initiated the nucleation processes of ZnO nanoparticles in the presence of alcohols of different size and polarity. It was established that the most stable ZnO–TEA monomer obtained in the presence of octanol possess stronger coordination ability which could replace weaker hydrogen bonds obtained in ethanol media. The higher chelating efficiency of TEA towards zinc with tetrahedral geometry is observed with the change of solvent from ethanol to octanol. The calculated value of the Gibbs free energy interaction obtained in nonpolar octanol suggested that the amount of especially stable ZnO–TEA(octanol) monomer with $\Delta G^*_{INT} = -62.50$ kcal mol^{-1} was found to be the main controlling parameters for both nucleation and growth of ZnO nanoparticles, being 10.5 kcal mol^{-1} more stable than ZnO–TEA(ethanol) monomer [9]. The formation of such completely enclosed structure of ZnO–TEA(octanol) monomer in nonpolar alcohol was a consequence of the exceptional flexibility of all three of TEA hydroxyl chains compared to ethanol media.

It is interesting to note that the precipitation of ZnO was delayed for at least 4 h (it occurred after 24 h of ageing) at the mole ratio [TEA]/[Zn(acac)$_2$] = 1:1] solely in octanol media, indicating the strong impact of three TEA chains in such media. On the other hand, the large capacity of the ZnO–TEA(octanol) monomer to attract other ZnO molecule when it's in excess ([TEA]/[Zn(acac)$_2$] = 1:2]) was observed. This was accompanied by the formation of the especially stable ZnO–TEA–ZnO(octanol) species with $\Delta G^*_{INT} = -63.2$ kcal mol^{-1}. The big difference in values of Gibbs free energies of ZnO–TEA molecular interactions revealed that the use of octanol as solvent leads to more spontaneous formation of ZnO–TEA monomers, as well as ZnO–TEA–ZnO species in comparison to ethanol solvent, which results in a higher nucleation rate of ZnO nuclei. The use of octanol as a nonpolar solvent leads to ZnO crystallites smaller than those obtained using polar ethanol (<10 nm).

The results of present investigation show the impact of surface interactions between the formed ZnO nanoparticles and the molecules of solvent and TEA on the way of growth and aggregation, which enables the control of their morphological properties.

Acknowledgments

This work has been partially supported by SAFU, project KK.01.1.1.01.0001.

The authors would like to thank the Zagreb University Computing Centre (SRCE) for generously granting computational resources on the ISABELLA cluster (isabella.srce.hr) and the CRO-NGI infra-structure (www.cro-ngi.hr).

Appendix A. Supplementary data

Supplementary data to this article can be found online at https://doi.org/10.1016/j.molstruc.2018.10.025.

References

[1] B. Ludi, M. Niederberger, Zinc oxide nanoparticles: chemical mechanisms and classical and non-classical crystallization, Dalton Trans. 42 (2013) 12554–12568, https://doi.org/10.1039/c3dt50610j.
[2] N. Pinna, G. Garnweitner, M. Antonietti, M. Niederberger, A general nonaqueous route to binary metal oxide nanocrystals involving a C–C bond cleavage, J. Am. Chem. Soc. 127 (2005) 5608–5612, https://doi.org/10.1021/ja042323r.
[3] G. Ambrožič, S.D. Škapin, M. Žigon, Z.C. Orel, The synthesis of zinc oxide nanoparticles from zinc acetylacetonate hydrate and 1-butanol or isobutanol, J. Colloid Interface Sci. 346 (2010) 317–323, https://doi.org/10.1016/j.jcis.2010.03.001.
[4] J. Park, J. Joo, S.G. Kwon, Y. Jang, T. Hyeon, Synthesis of monodisperse spherical nanocrystals, Angew. Chem. Int. Ed. Engl. 46 (2007) 4630–4660, https://doi.org/10.1002/anie.200603148.
[5] M.M. Demir, R. Muñoz-Espí, I. Lieberwirth, G. Wegner, Precipitation of monodisperse ZnO nanocrystals via acid-catalyzed esterification of zinc acetate, J. Mater. Chem. 16 (2006) 2940–2947, https://doi.org/10.1039/B601451H.
[6] X. Wang, Q. Zhang, Q. Wan, G. Dai, C. Zhou, B. Zou, Controllable ZnO architectures by ethanolamine-assisted hydrothermal reaction for enhanced photocatalytic activity, J. Phys. Chem. C 115 (2011) 2769–2775, https://doi.org/10.1021/jp1096822.
[7] R. Razali, A.K. Zak, W.H.A. Majid, M. Darroudi, Solvothermal synthesis of microsphere ZnO nanostructures in DEA media, Ceram. Int. 37 (2011) 3657–3663, https://doi.org/10.1016/j.ceramint.2011.06.026.
[8] A. Šarić, G. Štefanić, G. Dražić, M. Gotić, Solvothermal synthesis of zinc oxide microspheres, J. Alloys Comp. 652 (2015) 91–99, https://doi.org/10.1016/j.jallcom.2015.08.200.
[9] A. Šarić, I. Despotović, G. Štefanić, G. Dražić, The influence of ethanolamines on the solvothermal synthesis of zinc oxide: a combined experimental and theoretical study, ChemistrySelect 2 (2017) 10038–10049, https://doi.org/10.1002/slct.201701692.
[10] M. Niederberger, Nonaqueous sol–gel routes to metal oxide nanoparticles, Acc. Chem. Res. 40 (2007) 793–800, https://doi.org/10.1021/ar600035e.
[11] A. Šarić, M. Gotić, G. Štefanić, G. Dražić, Synthesis of ZnO particles using water molecules generated in esterification reaction, J. Mol. Struct. 1140 (2017) 12–18, https://doi.org/10.1016/j.molstruc.2016.10.057.
[12] J. Wojnarowicz, A. Opalinska, T. Chudoba, S. Gierlotka, R. Mukhovskyi, E. Pietrzykowska, K. Sobczak, W. Lojkowski, Effect of water content in ethylene glycol solvent on the size of ZnO nanoparticles prepared using microwave solvothermal synthesis, J. Nanomater. 2016 (2016), https://doi.org/10.1155/2016/2789871.
[13] J. Wojnarowicz, T. Chudoba, S. Gierlotka, K. Sobczak, W. Lojkowski, Size control of cobalt-doped ZnO nanoparticles obtained in microwave solvothermal synthesis, Crystals 8 (2018) 179, https://doi.org/10.3390/cryst8040179.
[14] J. Wojnarowicz, T. Chudoba, I. Koltsov, S. Gierlotka, S. Dworakowska, W. Lojkowski, Size control mechanism of ZnO nanoparticles obtained in microwave solvothermal synthesis, Nanotechnology 29 (2018) 065601, https://doi.org/10.1088/1361-6528/aaa0ef.
[15] P. Tonto, O. Mekasuwandumrong, S. Phatanasri, V. Pavarajarn, P. Praserthdam, Preparation of ZnO nanorod by solvothermal reaction of zinc acetate in various alcohols, Ceram. Int. 34 (2008) 57–62, https://doi.org/10.1016/j.ceramint.2006.08.003.
[16] Z. Hu, G. Oskam, P.C. Searson, Influence of solvent on the growth of ZnO nanoparticles, J. Colloid Interface Sci. 263 (2003) 454–460.
[17] G. Oskam, F. de J.P. Poot, Synthesis of ZnO and TiO$_2$ nanoparticles, J. Sol. Gel

Sci. Technol. 37 (2006) 157–160, https://doi.org/10.1007/s10971-005-6620-3.
[18] I. Bilecka, P. Elser, M. Niederberger, Kinetic and thermodynamic aspects in the microwave-assisted synthesis of ZnO nanoparticles in benzyl alcohol, ACS Nano 3 (2009) 467–477, https://doi.org/10.1021/nn800842b.
[19] Y. Inubushi, R. Takami, M. Iwasaki, H. Tada, S. Ito, Mechanism of formation of nanocrystalline ZnO particles through the reaction of [Zn(acac)2] with NaOH in EtOH, J. Colloid Interface Sci. 200 (1998) 220–227, https://doi.org/10.1006/jcis.1997.5354.
[20] M. Salavati-Niasari, F. Davar, Z. Fereshteh, Synthesis and characterization of ZnO nanocrystals from thermolysis of new precursor, Chem. Eng. J. 146 (2009) 498–502. https://doi.org/10.1016/j.cej.2008.09.042.
[21] M. Salavati-Niasari, F. Davar, A. Khansari, Nanospherical and nanobundles of ZnO: synthesis and characterization, J. Alloys Compd. 509 (2011) 61–65. https://doi.org/10.1016/j.jallcom.2010.08.060.
[22] A.K. Babaheydari, M. Salavati-Niasari, A. Khansari, Solvent-less synthesis of zinc oxide nanostructures from Zn(salen) as precursor and their optical properties, Particuology 10 (2012) 759–764. https://doi.org/10.1016/j.partic.2012.03.006.
[23] N. Mir, M. Salavati-Niasari, F. Davar, Preparation of ZnO nanoflowers and Zn glycerolate nanoplates using inorganic precursors via a convenient rout and application in dye sensitized solar cells, Chem. Eng. J. 181–182 (2012) 779–789. https://doi.org/10.1016/j.cej.2011.11.085.
[24] F. Soofivand, M. Salavati-Niasari, F. Mohandes, Novel precursor-assisted synthesis and characterization of zinc oxide nanoparticles/nanofibers, Mater. Lett. 98 (2013) 55–58. https://doi.org/10.1016/j.matlet.2013.01.129.
[25] F. Mazloom, M. Masjedi-Arani, M. Ghiyasiyan-Arani, M. Salavati-Niasari, Novel sodium dodecyl sulfate-assisted synthesis of $Zn_3V_2O_8$ nanostructures via a simple route, J. Mol. Liq. 214 (2016) 46–53. https://doi.org/10.1016/j.molliq.2015.11.033.
[26] G.K. Williamson, W.H. Hall, Acta Metall. 1 (1953) 22–31.
[27] Modern powder diffraction, in: D.L. Bish, J.E. Post (Eds.), Reviews in Mineralogy, Mineralogical society of America, Washington, 1989.
[28] M.J. Frisch, G.W. Trucks, H.B. Schlegel, G.E. Scuseria, M.A. Robb, J.R. Cheeseman, G. Scalmani, V. Barone, B. Mennucci, G.A. Petersson, H. Nakatsuji, M. Caricato, X. Li, H.P. Hratchian, A.F. Izmaylov, J. Bloino, G. Zheng, J.L. Sonnenberg, M. Hada, M. Ehara, K. Toyota, R. Fukuda, J. Hasegawa, M. Ishida, T. Nakajima, Y. Honda, O. Kitao, H. Nakai, T. Vreven, J.A. Montgomery Jr., J.E. Peralta, F. Ogliaro, M. Bearpark, J.J. Heyd, E. Brothers, K.N. Kudin, V.N. Staroverov, R. Kobayashi, J. Normand, K. Raghavachari, A. Rendell, J.C. Burant, S.S. Iyengar, J. Tomasi, M. Cossi, N. Rega, J.M. Millam, M. Klene, J.E. Knox, J.B. Cross, V. Bakken, C. Adamo, J. Jaramillo, R. Gomperts, R.E. Stratmann, O. Yazyev, A.J. Austin, R. Cammi, C. Pomelli, J.W. Ochterski, R.L. Martin, K. Morokuma, V.G. Zakrzewski, G.A. Voth, P. Salvador, J.J. Dannenberg, S. Dapprich, A.D. Daniels, Ö. Farkas, J.B. Foresman, J.V. Ortiz, J. Cioslowski, D.J. Fox, Gaussian 09, Revision D.01, Gaussian, Inc., Wallingford CT, 2009.
[29] Y. Zhao, N.E. Schultz, D.G. Truhlar, Design of density functionals by combining the method of constraint satisfaction with parametrization for thermochemistry, thermochemical kinetics, and noncovalent interactions, J. Chem. Theor. Comput. 2 (2006) 364–382, https://doi.org/10.1021/ct0502763.
[30] Y. Zhao, D.G. Truhlar, Density functionals with broad applicability in chemistry, Acc. Chem. Res. 41 (2008) 157–167, https://doi.org/10.1021/ar700111a.
[31] Y. Zhao, D.G. Truhlar, Density functional theory for reaction energies: test of meta and hybrid meta functionals, range-separated functionals, and other high-performance functionals, J. Chem. Theor. Comput. 7 (2011) 669–676, https://doi.org/10.1021/ct1006604.
[32] E.A. Amin, D.G. Truhlar, Zn coordination chemistry: development of benchmark suites for geometries, dipole moments, and bond dissociation energies and their use to test and validate density functionals and molecular orbital theory, J. Chem. Theor. Comput. 4 (2008) 75–85, https://doi.org/10.1021/ct700205n.
[33] C.J. Cramer, D.G. Truhlar, Density functional theory for transition metals and transition metal chemistry, Phys. Chem. Chem. Phys. 11 (2009) 10757–10816, https://doi.org/10.1039/b907148b.
[34] W.R. Wadt, P.J. Hay, Ab initio effective core potentials for molecular calculations. Potentials for main group elements Na to Bi, J. Chem. Phys. 82 (1985) 284–298, https://doi.org/10.1063/1.448800.
[35] A.V. Marenich, C.J. Cramer, D.G. Truhlar, J. Phys. Chem. B 113 (2009) 6378–6396.
[36] R.F.W. Bader, Atoms in Molecules: a Quantum Theory, Oxford University Press, Oxford, New York, 1994.
[37] T.A. Keith, AIMAll (Version 17.01.25), TK Gristmill Software, Overland Park KS, USA, 2017 (aim.tkgristmill.com).
[38] R.F.W. Bader, A bond path: a universal indicator of bonded interactions, J. Phys. Chem. A 102 (1998) 7314–7323, https://doi.org/10.1021/jp981794v.
[39] R.F.W. Bader, H. Essén, The characterization of atomic interactions, J. Chem. Phys. 80 (1984) 1943–1960, https://doi.org/10.1063/1.446956.
[40] D. Cremer, E. Kraka, A description of the chemical bond in terms of local properties of electron density and energy, Croat. Chem. Acta 57 (1984) 1259–1281.
[41] E. Espinosa, E. Molins, C. Lecomte, Hydrogen bond strengths revealed by topological analyses of experimentally observed electron densities, Chem. Phys. Lett. 285 (1998) 170–173, https://doi.org/10.1016/S0009-2614(98)00036-0.
[42] E. Espinosa, I. Alkorta, I. Rozas, J. Elguero, E. Molins, About the evaluation of the local kinetic, potential and total energy densities in closed-shell interactions, Chem. Phys. Lett. 336 (2001) 457–461, https://doi.org/10.1016/S0009-2614(01)00178-6.
[43] A.O. Borissova, M.Y. Antipin, H.A. Karapetyan, A.M. Petrosyan, K.A. Lyssenko, Cooperativity effects of H-bonding and charge transfer in an L-nitroarginine crystal with Z' > 1, Mendeleev Commun. 20 (2010) 260–262, https://doi.org/10.1016/j.mencom.2010.09.006.
[44] G.V. Baryshnikov, B.F. Minaev, V.A. Minaeva, V.G. Nenajdenko, Single crystal architecture and absorption spectra of octathio[8]circulene and *sym*-tetraselenatetrathio[8]circulene: QTAIM and TD-DFT approach, J. Mol. Model. 19 (2013) 4511–4519, https://doi.org/10.1007/s00894-013-1962-1.
[45] G.V. Baryshnikov, B.F. Minaev, A.A. Korop, V.A. Minaeva, A.N. Gusev, Structure of zinc complexes with 3-(pyridin-2-yl)-5-(arylideneiminophenyl)-1<Emphasis Type="Italic">H</Emphasis>-1,2,4-triazoles in different tautomeric forms: DFT and QTAIM study, Russ. J. Inorg. Chem. 58 (2013) 928–934, https://doi.org/10.1134/S0036023613080032.
[46] F. Shahangi, A.N. Chermahini, H. Farrokhpour, A. Teimouri, Selective complexation of alkaline earth metal ions with nanotubular cyclopeptides: DFT theoretical study, RSC Adv. 5 (2014) 2305–2317, https://doi.org/10.1039/C4RA08302D.
[47] L.N. Puntus, K.A. Lyssenko, M.Y. Antipin, J.-C.G. Bünzli, Role of inner- and outer-sphere bonding in the sensitization of EuIII-luminescence deciphered by combined analysis of experimental electron density distribution function and photophysical data, Inorg. Chem. 47 (2008) 11095–11107, https://doi.org/10.1021/ic801402u.
[48] J.S. Park, H.J. Hah, S.M. Koo, Y.S. Lee, Effect of alcohol chain length on particle growth in a mixed solvent system, J. Ceram. Process. Res. 7 (2006) 83.
[49] S. Sadasivan, A.K. Dubey, Y. Li, D.H. Rasmussen, Alcoholic solvent effect on silica synthesis—NMR and DLS investigation, J. Sol. Gel Sci. Technol. 12 (1998) 5–14, https://doi.org/10.1023/A:1008659708390.
[50] J. Dharma, A. Pisal, Application Note, Simple Method of Measuring the Band Gap Energy Value of TiO2 in the Powder Form Using a UV/Vis/NIR Spectrometer, Perkin-Elmer Inc, Shelton, CT., USA, 2009.
[51] B. Efafi, M. Sasani Ghamsari, M.A. Aberoumand, M.H. Majles Ara, H. Hojati Rad, Highly concentrated ZnO sol with ultra-strong green emission, Mater. Lett. 111 (2013) 78–80, https://doi.org/10.1016/j.matlet.2013.08.035.